Charge-transfer contribution to surface-enhanced Raman scattering in a molecular junction: Time-dependent correlations

Tae-Ho Park* and Michael Galperin†

Department of Chemistry and Biochemistry, University of California at San Diego, La Jolla, California 92093, USA

(Received 5 January 2011; revised manuscript received 11 July 2011; published 10 August 2011)

Raman spectroscopy of molecular junctions is a promising diagnostic and control tool. We present a model for charge-transfer contribution to surface-enhanced Raman spectroscopy, generalizing previous considerations to strong laser pulses of arbitrary time dependence. The approach paves a way to realistic simulations of Raman spectroscopy experiments in molecular junctions. We demonstrate that the optical response of molecular conduction junctions is correlated with the electron transport. Feynman diagrams responsible for such similarity are analyzed, and a possible explanation for observed (anti)correlated behavior of Stokes signal and conductance is proposed.

DOI: 10.1103/PhysRevB.84.075447 PACS number(s): 85.65.+h, 33.20.Fb, 78.20.Jq, 78.67.−n

I. INTRODUCTION

Surface enhancement of Raman spectroscopy for molecules chemisorbed on metal surfaces has been observed[1–4] and explained by a combination of local surface plasmon resonance (LSPR) of the metal[5,6] and charge transfer (CT) between the molecule and the metal.[7–14] Recent advancements in experimental techniques allowed measurement of optical response in molecular junctions. In particular, simultaneous measurement of electronic conductance and Raman response was reported in Resf. 15–17 use Raman spectroscopy for observation of heating in current-carrying junctions.

Like older "standard" spectroscopies (resonant[18,19] and off-resonant[20–24] inelastic electron tunneling spectroscopy, and noise spectroscopy[25]), junction optical spectroscopies are expected to play important roles in the field of molecular electronics both as diagnostic methods and as control tools for molecular devices. Optical spectroscopy at equilibrium is well established.[26] Optical spectroscopy of current-carrying junctions sets a theoretical challenge in the need to describe the optical response of an open nonequilibrium molecular system.

Recently, a theory of Raman scattering in molecular junction, modeled by two levels [highest occupied molecular orbital (HOMO) and lowest unoccupied molecular orbital (LUMO) or ground and excited states] attached to metallic electrodes, was considered within nonequilibrium Green's function (NEGF) formulation.[27,28] This consideration is restricted to mostly resonant Raman scattering in a junction under steady-state conditions. With most of the experimental measurements performed for the off-resonant situation, two theoretical approaches were proposed: (i) the same two-level model was employed within the quantum master equation (QME) approach to calculate junction polarizability[29] and (ii) the single-level model for charge-transfer contribution to surface-enhanced Raman spectroscopy (SERS) at equilibrium introduced in Ref. 8 was generalized to the steady-state junction situation within NEGF.[30] Since standard QME misses essential junction information (see, e.g., Refs. 31 and 32 for discussion), the latter development is more promising. Note, however, that the incident field in both Refs. 8 and 30 is treated at second order of perturbation theory, which is questionable for strongly enhanced local fields detected in experiments. Treating the incident field classically in nonperturbative manner is more relevant for SERS. Also, explicit time dependency of the driving field can be easily incorporated into the model. This, together with developed approaches for time-dependent transport within NEGF,[33–38] paves a way to practical formulation of a scheme capable of simulation of time-dependent Raman scattering in realistic molecular junctions.

Here, we consider a model for non-resonant Raman spectroscopy in molecular junctions, generalizing consideration of Ref. 30 to non-perturbative treatment of driving laser field with possibility to include explicit time dependence of the latter into consideration. Section II introduces our model and discusses the approach used to simulate off-resonant vibrational Raman signal. Application of the approach to the analytically solvable case of single harmonic mode is considered in Sec. III. Numerical examples and discussion of correlation between Raman flux and junction conductance are given in Sec. IV. Section V concludes and outlines directions for future research.

II. MODEL

We consider a molecule (M) coupled to two metallic contacts (L and R), reservoirs of free charge carriers each at its own equilibrium, and a bath of free radiation (accepting) modes. Contacts induce an electric current (electron transfer between the molecule and contacts) across the junction. The radiation bath represents the device measuring outgoing photon flux. The molecule is modeled by a single level ε_0 coupled to a single molecular vibration and driven by an external (classical) electromagnetic field (pumping mode). The Hamiltonian of the system is

$$\hat{H}(t) = \hat{H}_0(t) + \hat{V}, \tag{1}$$

$$\hat{H}_0(t) = \hat{H}_M(t) + \hat{H}_K + \hat{H}_p, \tag{2}$$

$$\hat{V} = \hat{V}_{et} + \hat{V}_p. \tag{3}$$

Here, $\hat{H}_K$ $(K = L, R)$, $\hat{H}_p$ are contacts and radiation-bath Hamiltonians

$$\hat{H}_K = \sum_{k\in K} \varepsilon_k \hat{c}_k^\dagger \hat{c}_k, \tag{4}$$

$$\hat{H}_p = \sum_f \nu_f \hat{a}_f^\dagger \hat{a}_f, \tag{5}$$

where $\hat{c}_k^\dagger$ ($\hat{c}_k$) is an operator of creation (annihilation) of an electron in state k of the contact, and $\hat{a}_f^\dagger$ ($\hat{a}_f$) creates (annihilates) a photon in state f of the radiation bath. The molecular Hamiltonian is

$$\hat{H}_M(t) = [\varepsilon_0 - \mu E(t)]\,\hat{d}^\dagger\hat{d} + \omega_v \hat{v}^\dagger\hat{v} + M_v(\hat{v}+\hat{v}^\dagger)\hat{d}^\dagger\hat{d}, \quad (6)$$

where $\hat{d}^\dagger$ ($\hat{d}$) is a creation (annihilation) operator for an electron on the level ε_0, $E(t)$ is an external driving field, μ is the projection of the molecular dipole moment to the direction of the external field, $\hat{v}^\dagger$ ($\hat{v}$) creates (annihilates) a phonon in a molecular vibration, and M_v characterizes coupling between a tunneling electron and the vibration. Finally, $\hat{V}_{et}$ and $\hat{V}_p$ couple the molecule to contacts and the radiation bath

$$\hat{V}_{et} = \sum_{k\in\{L,R\}} (V_k \hat{d}^\dagger \hat{c}_k + \text{H.c.}), \quad (7)$$

$$\hat{V}_p = \sum_f M_f(\hat{a}_f + \hat{a}_f^\dagger)\hat{d}^\dagger\hat{d}. \quad (8)$$

This model is a generalization of the SERS model considered previously.[8,30] Note that molecular Hamiltonian (6) can be represented in a more general form (e.g., in terms of Hubbard operators) with an appropriate change in the methodology to calculate Raman scattering and current in the junction (see Ref. 40 for details).

Time-dependent current at interface K (L or R) is calculated with the usual NEGF expression[33]

$$I_K(t) = 2\,\text{Re}\int_{-\infty}^{t} dt'[\Sigma_K^<(t,t')\,G^>(t',t) - \Sigma_K^>(t,t')\,G^<(t',t)]. \quad (9)$$

Here, $\Sigma_K^{>(<)}(t,t')$ is a greater (lesser) projection of an electronic self-energy due to coupling to contact K:

$$\Sigma_K(\tau,\tau') = \sum_{k\in K} |V_k|^2 g_k(\tau,\tau'), \quad (10)$$

where τ (τ') is the contour variable corresponding to the real time t (t'), and

$$g_k(\tau,\tau') = -i\langle T_c\,\hat{c}_k(\tau)\,\hat{c}_k^\dagger(\tau')\rangle \quad (11)$$

is the Green's function of a free electron in state k. In this model, we assume that time-dependent driving is confined to the molecular region only, so that projections of the contact self-energies depend on the difference of times, and Fourier transform yields the familiar result

$$\Sigma_K^<(E) = i\Gamma_K(E) f_K(E), \quad (12)$$

$$\Sigma_K^>(E) = -i\Gamma_K(E)\,[1 - f_K(E)]\,. \quad (13)$$

Here, $f_K(E) = [e^{(E-\mu_K)/T}+1]^{-1}$ is the Fermi distribution in a contact K, and

$$\Gamma_K(E) = \sum_{k\in K} |V_k|^2 \delta(E-\varepsilon_k) \quad (14)$$

is the escape rate from a molecular level into the contact K. In what follows, we assume wide-band approximation[41] treating Γ_K as an energy-independent quantity.

$G^{>(<)}(t,t')$ in Eq. (9) is the greater (lesser) projection of the single-particle Green's function

$$G(\tau,\tau') = -i\langle T_c\,\hat{d}(\tau)\,\hat{d}^\dagger(\tau')\rangle. \quad (15)$$

To calculate the time-dependent Raman flux, we follow the argument of Refs. 27, 28, and 30. Raman flux into a mode f is assumed to be an outgoing photon flux from the system into the mode resulting from coherent scattering process. Bose (photon) flux from the molecular system into mode f is (derivation is similar to the heat-flux derivation presented in Appendix A of Ref. 42)

$$J_f(t) = -\frac{|M_f|^2}{\nu_f}\text{Re}\int_{-\infty}^{t} dt_1 \left[\frac{\partial}{\partial t_1}(D_f^<(t,t_1))\mathcal{G}^>(t_1,t) - \frac{\partial}{\partial t_1}(D_f^>(t,t_1))\mathcal{G}^<(t_1,t)\right]. \quad (16)$$

Here, $D_f^{>(<)}(t,t')$ is the greater (lesser) projection of the free-photon Green's function in a mode f:

$$D_f(\tau,\tau') = -i\langle T_c\,\hat{Q}_f(\tau)\,\hat{Q}_f^\dagger(\tau')\rangle, \quad (17)$$

where $\hat{Q}_f = \hat{a}_f + \hat{a}_f^\dagger$, and $\mathcal{G}^{>(<)}(t,t')$ is a greater (lesser) projection of the two-particle (two-time) electron Green's function

$$\mathcal{G}(\tau,\tau') = -\langle T_c\,\hat{n}(\tau)\,\hat{n}(\tau')\rangle, \quad (18)$$

where $\hat{n} = \hat{d}^\dagger\hat{d}$. Since the radiation bath is a set of free empty modes, i.e.,

$$D_f^<(t,t') = -ie^{+i\nu_f(t-t')}, \quad (19)$$

$$D_f^>(t,t') = -ie^{-i\nu_f(t-t')}, \quad (20)$$

and

$$\mathcal{G}^>(t,t') = \mathcal{G}^<(t',t) = [\mathcal{G}^<(t,t')]^*. \quad (21)$$

Equation (16) leads to

$$J_f(t) = 2|M_f|^2\text{Re}\int_{-\infty}^{t} dt'\,e^{i\nu_f(t-t')}\mathcal{G}^<(t,t'). \quad (22)$$

Note that Eq. (22) yields time-dependent Raman flux when only coherent electron scattering events are considered in $\mathcal{G}^<(t,t')$.

Time-dependent current [Eq. (9)] and Raman flux [Eq. (22)] can be calculated when the single-electron [Eq. (15)] and the two-electron [Eq. (18)] Green's functions are known. These Green's functions should take into account interactions with incident field $E(t)$, contacts L and R, radiation bath $\{f\}$, and molecular vibration v. Within the models (1)–(8), the interaction with the pumping field is taken into account nonperturbatively: $E(t)$ enters the molecular time-dependent Hamiltonian (6) explicitly as a driving force. We assume that, in the absence of the laser pulse, the molecular junction is in a bias-induced steady state, and consider the coupling to contacts included into "zeroth-order Hamiltonian." Thus, interactions with the radiation bath and molecular vibration are treated as perturbations to the unperturbed molecular junction. Taking into account that the radiation bath represents a measuring device for outgoing photon flux, i.e., it counts and absorbs photons, second order in coupling to the bath is adequate to

represent the physics. Coupling to the molecular vibration can be treated at different levels of sophistication, including the dressed-states picture with Hubbard NEGF (Ref. 40) or generalized QME (Refs. 31 and 32) approaches. Below (for illustration purposes only and to keep discussion simple), we restrict this treatment to second order in electron-vibration coupling. It was shown in Ref. 30 that the main contribution to the Raman process in this case comes from the particle-particle (or particle-hole) scattering processes [see example of a diagram in Fig. 1(a)]. This leads to the expression for the time-dependent Raman flux in the form

$$J_f(t) = 2|M_f|^2|M_v|^2 \mathrm{Im}\int_{-\infty}^{t} dt' e^{i\nu_f(t-t')} \times \int_{-\infty}^{+\infty} dt_1 \int_{-\infty}^{+\infty} dt_2\, P^r(t,t_1)\, D_v^<(t_1,t_2)\, P^a(t_2,t'), \tag{23}$$

where r, $<$, and a stand for retarded, lesser, and advanced projection, respectively, of the electron bubble diagram

$$P(\tau_1,\tau_2) = -iG(\tau_1,\tau_2)\, G(\tau_2,\tau_1), \tag{24}$$

and the phonon Green's function

$$D_v(\tau_1,\tau_2) = -i\langle T_c\, \hat{Q}_v(\tau_1)\, \hat{Q}_v(\tau_2)\rangle. \tag{25}$$

Here, $\hat{Q}_v = \hat{v} + \hat{v}^\dagger$. Below, for simplicity we treat vibration as a free phonon. The lesser projection of the free-phonon Green's function is

$$D_v^<(t_1,t_2) = -i(N_v e^{-i\omega_v(t_1-t_2)} + [1+N_v]e^{i\omega_v(t_1-t_2)}), \tag{26}$$

where $N_v = [e^{\hbar\omega_v/T} - 1]^{-1}$ is the Bose-Einstein thermal distribution.

Raman spectroscopy measures the flux of outgoing photons resulting from the electron scattering. It is reasonable to expect that the energetics (spectrum) of the former may be at least partially similar to the energetics (spectrum) of the latter. Indeed, inelastic electron tunneling spectroscopy is an example of obtaining information on vibrational degrees of freedom through electric current measurements. For example, recently, a similar argument was used to show that phonon spectroscopy for a double quantum dot locally coupled to the molecular vibration can be measured by the electric conductance.[43] The electron participating in the Raman scattering event may contribute to the current (conductance) in the molecular junction. Clearly, the current has contributions also from electrons undergoing other scattering events (elastic scattering, inelastic scattering on molecular vibration, scattering by pumping mode only), however, with appropriate choice of the molecular level position relative to Fermi energy in the contacts, one may hope to observe contribution to current mostly from Raman scattered electrons.

Experimental data on simultaneous measurements of Raman scattering and conductance show correlation between optical and transport properties in molecular junctions.[15] Explanation of the effect used in Ref. 15 is based on the assumption that the molecule changes its conformation under laser pulse. While such a scenario is reasonable and indeed may explain the effect, here we propose an alternative explanation, which may also be relevant.

Electron-electron (electron-hole) scattering events contributing to the Raman diagram [Fig. 1(a)] are presented in Fig. 1(b). One can obtain those three scattering diagrams by cutting two of four electron lines in Fig. 1(a). These scattering events contribute to single-particle self-energy terms shown in Fig. 1(c). The self-energies provide information on energetics of the Raman scattering process in the electric current. Among four diagrams presented in Fig. 1(c), the dominant contribution for the electric current is given by two rainbow diagrams (top row), while the others (diagrams in parentheses) are negligible. Corresponding contributions to the electron self-energy on the Keldysh contour are

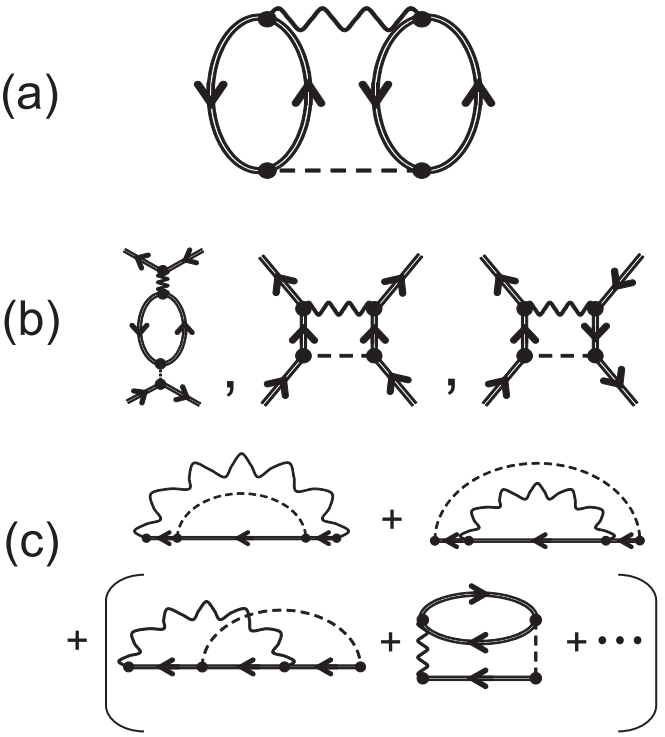

FIG. 1. Feynman diagrams for (a) Raman scattering, (b) related two-particle scattering process, and (c) fourth-order perturbation terms for electronic self-energy. Solid, dashed, and wavy lines describe electron propagation associated with an incident light field and coupling to contacts, propagation of outgoing photon, and phonon of the molecular vibration, respectively.

$$\Sigma_{ivf}(\tau_1,\tau_2) = -|M_v|^2 \int_0^\infty d\nu_f \rho(\nu_f)|M_f|^2 \times[\mathcal{F}_{ivf}(\tau_1,\tau_2) + \mathcal{F}_{ifv}(\tau_1,\tau_2)], \tag{27}$$

where

$$\mathcal{F}_{ivf(ifv)}(\tau_1,\tau_2) \equiv D_{v(f)}(\tau_1,\tau_2) \int_c d\tau_3 \int_c d\tau_4\, D_{f(v)}(\tau_3,\tau_4) \times G(\tau_1,\tau_3)G(\tau_3,\tau_4)G(\tau_4,\tau_2). \tag{28}$$

Here, $G(\tau,\tau')$ is the single-particle Green's function defined in Eq. (15), $D_f(\tau,\tau')$ and $D_v(\tau,\tau')$ are photon and phonon Green's functions defined in Eqs. (17) and (25), respectively, and

$$\rho(\nu_f) = \frac{\nu_f^2}{\pi^2 c^3} e^{-\nu_f/\nu_c} \tag{29}$$

is the optical density of the radiation bath (c is the speed of light and ν_c is the cutoff frequency). Note that the

single-particle Green's function $G(\tau,\tau')$ in (28) takes into account coupling between molecule and contacts, and external driving by construction.

Additional (lower order in interaction) contributions to the current (not related to Raman spectroscopy) that we consider are elastic, inelastic, and Rayleigh scatterings. Self-energy corresponding to the elastic scattering is defined in Eq. (10), Rayleigh scattering yields

$$\Sigma_{if}(\tau_1,\tau_2) = i\int_0^\infty d\nu_f \rho(\nu_f)|M_f|^2 G(\tau_1,\tau_2)D_f(\tau_1,\tau_2), \tag{30}$$

and inelastic effects are treated within the second Born approximation

$$\Sigma_{iv}(\tau_1,\tau_2) = i|M_v|^2 G(\tau_1,\tau_2)D_v(\tau_1,\tau_2) \tag{31}$$

to be consistent with the level of theory (second-order perturbation theory) used in treating Raman process [see Fig. 1(a)].

The total self-energy is

$$\Sigma(\tau_1,\tau_2) = \sum_{K=L,R}\Sigma_K(\tau_1,\tau_2) + \Sigma_{iv}(\tau_1,\tau_2) + \Sigma_{if}(\tau_1,\tau_2) + \Sigma_{ivf}(\tau_1,\tau_2). \tag{32}$$

Lesser and greater projections of the single-electron Green's function needed to calculate the current [Eq. (9)] are obtained from the Keldysh equation[44]

$$G^{\lessgtr}(t,t') = \int_{-\infty}^{+\infty} dt_1 \int_{-\infty}^{+\infty} dt_2\, G^r(t,t_1)\,\Sigma^{\lessgtr}(t_1,t_2)\,G^a(t_2,t'). \tag{33}$$

The additive structure of the self-energy [Eq. (32)] upon substitution to Eqs. (33) and (9) leads to an additive expression for the time-dependent current

$$I_K(t) = I_K^i(t) + I_K^{iv}(t) + I_K^{if}(t) + I_K^{ivf}(t), \tag{34}$$

where

$$I_K^x(t) = 2\,\mathrm{Re}\int_{-\infty}^{t} dt' \int_{-\infty}^{+\infty} dt_1 \int_{-\infty}^{+\infty} dt_2 \times [\Sigma_K^<(t,t')\,G^r(t',t_1)\,\Sigma_x^>(t_1,t_2)\,G^a(t_2,t) - \Sigma_K^>(t,t')\,G^r(t',t_1)\,\Sigma_x^<(t_1,t_2)\,G^a(t_2,t)] \tag{35}$$

with $x \in \{L+R, iv, if, ivf\}$. This concludes the description of procedure to simulate time-dependent Raman and current in the molecular junction for our model.

III. HARMONIC DRIVING

Electric field $E(t)$ in molecular Hamiltonian $\hat{H}_M$ [Eq. (6)] is a local field formed by response of surface plasmons to an incident laser beam. Areas of high local field intensity ("hot spots") make detection of molecular optical response feasible.[45] Tools of classical electrodynamics may be employed to simulate time dependency of a local field.[38,39] By treating the latter as a driving force, one can get the time-dependent Raman signal and charge flux within the approach described above.

To make analytical progress possible, here we restrict our consideration to harmonic driving

$$E(t) = E_0\cos(\nu_i t), \tag{36}$$

where ν_i is the frequency of the incident wave. In this case, analytic expressions for projections of the single-particle Green's functions (15) are[33]

$$G^r(t,t') = -i\theta(t-t')\exp\left\{-i\left(\varepsilon_0 - i\frac{\Gamma}{2}\right)(t-t') - i\frac{C}{\nu_i}[\sin(\nu_i t) - \sin(\nu_i t')]\right\}, \tag{37}$$

$$G^{\lessgtr}(t,t') = \sum_{k_1,k_2=-\infty}^{\infty} J_{k_1}\left(\frac{C}{\nu_i}\right) J_{k_2}\left(\frac{C}{\nu_i}\right)\int\frac{dE}{2\pi}\Sigma_{L+R}^{\lessgtr}(E) \times \frac{e^{-i\frac{C}{\nu_i}[\sin(\nu_i t)-\sin(\nu_i t')]}e^{-i[E(t-t')-\nu_i(k_1 t-k_2 t')]}}{\left[E-\varepsilon_0-k_1\nu_i+i\frac{\Gamma}{2}\right]\left[E-\varepsilon_0-k_2\nu_i-i\frac{\Gamma}{2}\right]}, \tag{38}$$

where $\Gamma = \Gamma_L + \Gamma_R$, $C = \mu E_0$, $\theta(t-t')$ is the Heaviside step function, and $\Sigma_{L+R}^{\lessgtr} = \Sigma_L^{\lessgtr} + \Sigma_R^{\lessgtr}$. Derivation of Eq. (38) employed the identity

$$\exp\left[i\frac{C}{\nu_i}\sin(\nu_i t)\right] = \sum_{k=-\infty}^{+\infty} e^{i\nu_i k t} J_k\left(\frac{C}{\nu_i}\right), \tag{39}$$

where J_k is Bessel function of the first kind.[46]

Substituting (37) and (38) into (23), one gets for the time-dependent Raman flux

$$J_f(t) = 2|M_f|^2|M_v|^2\,\mathrm{Im}\int_{-\infty}^{t} dt' e^{i\nu_f(t-t')}[N_v P^r(t,\omega_v)P^a \times(\omega_v,t') + [N_v+1]P^r(t,-\omega_v)P^a(-\omega_v,t')], \tag{40}$$

where

$$P^r(t,\omega) = \int_{-\infty}^{+\infty} dt' P^r(t,t')e^{-i\omega t'} \tag{41}$$

$$= -i\sum_{k_1,k_2=-\infty}^{\infty} J_{k_1}\left(\frac{C}{\nu_i}\right) J_{k_2}\left(\frac{C}{\nu_i}\right) e^{-i[\omega+(k_2-k_1)\nu_i]t}\int\frac{dE}{2\pi}\frac{\Sigma_{L+R}^<(E)}{\left[E-\varepsilon_0-k_1\nu_i+i\frac{\Gamma}{2}\right]\left[E-\varepsilon_0-k_2\nu_i-i\frac{\Gamma}{2}\right]} \times\left(\frac{1}{E-\varepsilon_0-k_1\nu_i+\omega+i\frac{\Gamma}{2}} + \frac{1}{E-\varepsilon_0-k_2\nu_i-\omega-i\frac{\Gamma}{2}}\right) \tag{42}$$

is the right-side Fourier transform of the retarded projection of the electron bubble diagram [Eq. (24)] and $P^a(E,t') = [P^r(t',E)]^*$. Averaging (40) over a period of the Raman-flux oscillation yields an energy conservation condition.

Electric current is calculated substituting (37) and (38) into lesser and greater projections of (27), (30), and (31), and using resulting expressions in (34) and (35). This yields the following expressions for time-averaged (over an oscillation period) contributions to the current:

$$\left\langle I_K^i(t)\right\rangle = 2\sum_\xi \int \frac{dE}{2\pi}\left|\sum_k \frac{J_k\left(\frac{C}{\nu_i}\right)J_{k-\xi}\left(\frac{C}{\nu_i}\right)}{E-\varepsilon_0+(\xi-k)\nu_i+i\frac{\Gamma}{2}}\right|^2 [\Sigma_K^<(E)\Sigma_{\bar K}^>(E+\xi\nu_i)-\Sigma_{\bar K}^<(E)\Sigma_K^>(E+\xi\nu_i)], \tag{43}$$

$$\begin{aligned}\left\langle I_K^{iv}(t)\right\rangle = {} & 2|M_v|^2\sum_\xi\int\frac{dE}{2\pi}\{N_v\Lambda_\xi(\omega_v,E)[\Sigma_K^<(E)\Sigma_{\bar K}^>(E+\omega_v+\xi\nu_i)-\Sigma_{\bar K}^<(E)\Sigma_K^>(E+\omega_v+\xi\nu_i)]\\ & +[N_v+1]\,\Lambda_\xi(-\omega_v,E)[\Sigma_K^<(E)\Sigma_{\bar K}^>(E-\omega_v+\xi\nu_i)-\Sigma_{\bar K}^<(E)\Sigma_K^>(E-\omega_v+\xi\nu_i)]\},\end{aligned} \tag{44}$$

$$\left\langle I_K^{if}(t)\right\rangle = 2|M_f|^2\sum_\xi\int_0^\infty d\nu_f\,\rho(\nu_f)\int\frac{dE}{2\pi}\,\Lambda_\xi(-\nu_f,E)[\Sigma_K^<(E)\Sigma_{\bar K}^>(E-\nu_f+\xi\nu_i)-\Sigma_{\bar K}^<(E)\Sigma_K^>(E-\nu_f+\xi\nu_i)], \tag{45}$$

$$\begin{aligned}\left\langle I_K^{ivf}(t)\right\rangle = {} & 2|M_v|^2\,|M_f|^2\mathrm{Re}\sum_\xi\int_0^\infty d\nu_f\,\rho(\nu_f)\int\frac{dE}{2\pi}\{N_v\left[\Phi_\xi^0(\omega_v,-\omega_v,E)+\Phi_\xi^0(\omega_v,\nu_f,E)\right]\\ & \times[\Sigma_K^<(E)\Sigma_{\bar K}^>(E+\omega_v-\nu_f+\xi\nu_i)-\Sigma_{\bar K}^<(E)\Sigma_K^>(E+\omega_v-\nu_f+\xi\nu_i)]\\ & +[N_v+1]\left[\Phi_\xi^0(-\omega_v,\omega_v,E)+\Phi_\xi^0(-\omega_v,\nu_f,E)\right]\\ & \times[\Sigma_K^<(E)\Sigma_{\bar K}^>(E-\omega_v-\nu_f+\xi\nu_i)-\Sigma_{\bar K}^<(E)\Sigma_K^>(E-\omega_v-\nu_f+\xi\nu_i)]\},\end{aligned} \tag{46}$$

where $\bar K$ stands for the alternative to the K choice of the the interface, and

$$\Lambda_\xi^0(x,E) \equiv \left|\sum_k \frac{J_k\left(\frac{C}{\nu_i}\right)J_{k-\xi}\left(\frac{C}{\nu_i}\right)}{\left[E-\varepsilon_0+x+(\xi-k)\nu_i+i\frac{\Gamma}{2}\right]\left[E-\varepsilon_0+(\xi-k)\nu_i+i\frac{\Gamma}{2}\right]}\right|^2, \tag{47}$$

$$\Phi_\xi^0(x,y,E) \equiv \left|\sum_k \frac{J_k\left(\frac{C}{\nu_i}\right)J_{k-\xi}\left(\frac{C}{\nu_i}\right)}{\left[E-\varepsilon_0+x-\nu_f+(\xi-k)\nu_i+i\frac{\Gamma}{2}\right]\left[E-\varepsilon_0-y+(\xi-k)\nu_i+i\frac{\Gamma}{2}\right]\left[E-\varepsilon_0+(\xi-k)\nu_i+i\frac{\Gamma}{2}\right]}\right|^2. \tag{48}$$

As in the case of Raman scattering, time averaging yields energy conservation conditions, which provide the enhancement of a contribution at the resonance of corresponding process. For example, I_K^{iv} has resonances when energy of the tunneling electron is detuned from ε_0 by $|\nu_i-\omega_v|$ or ω_v, which corresponds to inelastic tunneling with or without interaction with driving field. Below, we discuss results of numerical simulations of Raman flux [Eq. (40)] and current [Eqs. (43)–(46)] in the biased molecular junction subjected to the harmonic driving.

IV. NUMERICAL RESULTS

We present results of simulations of Stokes response and current for the models (1)–(8) under the harmonic driving (36) averaged over the period of oscillation. Parameters of the calculations (in units of Γ) are $T = 0.1$, $\nu_i = 20$, $\omega_v = 5$, $M_f = M_v = \sqrt{2}$, and $\nu_c = 25$. The positions of molecular level ε_0 and bias V_{sd} are indicated for each calculation. We take Fermi energy $E_F = 0$, and apply bias in a symmetric way, i.e., $\mu_{L,R} = \pm eV_{sd}/2$.

Figure 2 compares Stokes intensities calculated from Eq. (40) to the expressions presented in Ref. 30. The latter is based on perturbative treatment of coupling to driving mode, contrary to our approach treating this coupling exactly. Figure 2(a) shows the dependence of Stokes signal on position of molecular level. Both our approach and that of Ref. 30 give here similar results. The Stokes signal is symmetric around Fermi energy due to particle-hole symmetry preserved by the model.

Positions of the Stokes signal peaks at $\varepsilon_0 - E_F = \pm\omega_v$, $\pm(\nu_i-\omega_v)$, and $\pm\nu_i$ [see Fig. 2(a)] can be explained using the sketches in Fig. 3. Coupling between molecule and contact(s) leads to broadening of the molecular level, represented within the model as a Lorentzian centered at the position of the level. One can consider the Lorentzian as a continuum of independent levels. Presence of the molecular vibrational degree of freedom allows us to dress each molecular electronic level from this continuum with vibrational states. The latter are indicated by parabolas in Fig. 3 as states of harmonic oscillator. Electron Stokes scattering is a coherent process starting, say, at vibrationally ground state and ending at the

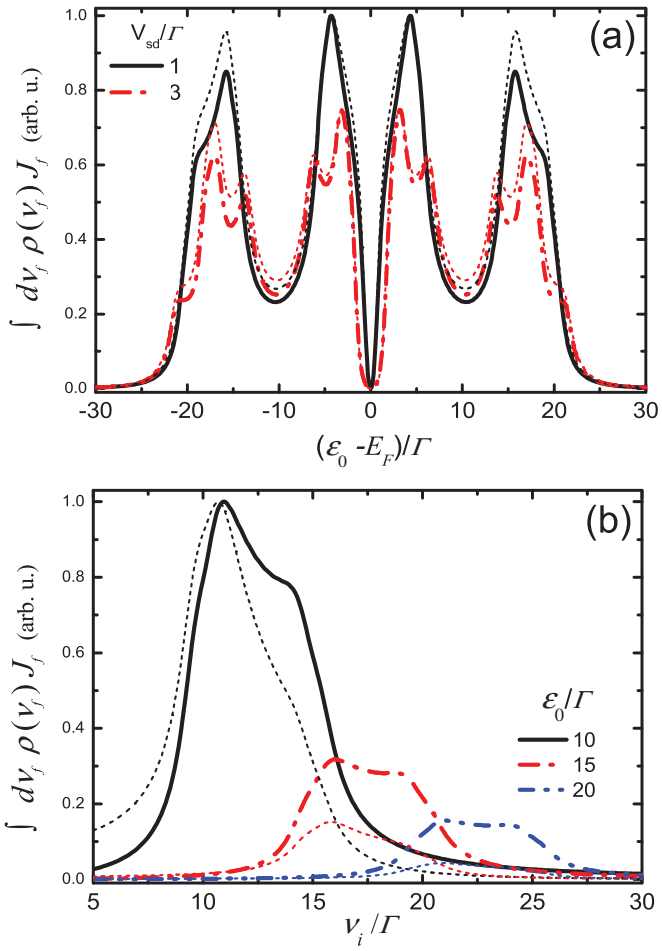

FIG. 2. (Color online) Stokes intensity averaged over period of oscillation of the photon flux [Eq. (40)] shown as a function of (a) the molecular level ε_0 position at $V_{sd} = 1$ (solid line, black) and 3 (dashed-dotted line, red) and (b) frequency of the incident laser field v_i at the level position $\varepsilon_0 = 10$ (solid line, black), 15 (dashed-dotted line, red), and 20 (dashed-double dotted line, blue). Results of Eq. (40) are compared with the perturbative method of Ref. 30 (dotted lines). See text for parameters.

first vibrationally excited state of some filled level from the continuum. The intermediate state of the scattering process is a level (or several levels) from the empty part of the continuum. For $E_F - \varepsilon_0 > v_i$, Raman scattering is impossible since an intermediate state is not empty. At $E_F - \varepsilon_0 \sim v_i$ [around -20

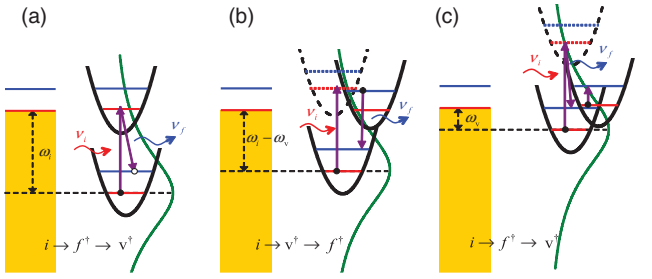

FIG. 3. (Color online) Sketches of the processes responsible for peaks in the Stokes intensity [Fig. 2(a)], located at (a) $E_F - \varepsilon_0 = \pm v_i$ (± 20), (b) $\pm(v_i - \omega_v)$ (± 15), and (c) $\pm\omega_v$ (± 5).

in Fig. 2(a)], the Stokes scattering becomes possible. The corresponding threshold is illustrated in a sketch in Fig. 3(a).

After crossing this threshold, two processes compete for the electron at the intermediate (excited) level: Raman scattering and electron transfer from molecule into contacts. As a result, the intensity of Raman signal due to this process should go down. However, an additional channel for Raman scattering opens at this point. This channel is a scattering process where electron returning back into the ground state comes from a different (not initially excited) intermediate level, which is ω_v lower in energy in the Lorentzian than the initially excited one [see sketch in Fig. 3(b)]. For the Stokes signal, this transition comes from a vibrationally excited state. This additional process leads to an increase in Stokes signal in the range of $E_F - \varepsilon_0$ from v_i to $v_i - \omega_v$. At the latter point, the channel closes since the level returning the electron to the ground state crosses the Fermi energy, becoming unpopulated. This leads to a decrease in Stokes signal for positions of ε_0 closer to E_F, which results in a peak in Fig. 2(a) at ~ -15.

A similar process occurs with involvement of a level shifted by ω_v from the initial level at ε_0 [see sketch in Fig. 3(c)]. Threshold behavior of the former leads to a peak at $E_F - \varepsilon_0 = \omega_v$ [~ -5 in Fig. 2(a)]. Note that peaks for level positions above Fermi energy $\varepsilon_0 > E_F$ can be explained along the same lines, considering the hole in place of particle transport. Note also that bias (two different chemical potentials on the two sides of the junction) smears and (at higher biases, $V_{sd} > \Gamma$) splits the peaks.

The difference between results of our approach from those of Ref. 30 are more pronounced in Fig. 2(b), where the Stokes signal is plotted as a function of incident field frequency. Our approach takes into account multiphoton processes absent in the perturbative treatment of original Persson's model[8] and its generalization.[30]

Figure 4 presents current [Eqs. (34) and (43)–(46)] as a function of level position ε_0 (a) and incident frequency v_i (b) under harmonic driving. Due to the presence of a driving force, the central ($\varepsilon_0 = E_F$) peak in the current versus level position dependence [see Fig. 4(a)] may come from any of the (43)–(46) contributions since elastic and inelastic (in vibrational degree of freedom or in outgoing photon) channels are always open in this case (note $v_i > \omega_v$ and most of v_f). Other peaks are mostly due to inelastic processes of I_K^i and I_K^{iv} [Eqs. (43) and (44)] and contributions to the current from the processes that determine similar structure in Stokes intensity versus the ε_0 plot [see Fig. 2(a)]. The latter comes from the I_K^{ivf} term [Eq. (46)].

There is an important difference between contributions of the Raman scattering processes into the Stokes intensity and charge flux. This difference is illustrated with the sketches presented in Fig. 5. Here, the Raman scattering process of Fig. 3(b) is shown for two different positions of ε_0 relative to contact Fermi energy. Both situations will contribute to Stokes intensity as is discussed above. However, only one of them will increase the charge flux through the junction. This difference in contributions explains the difference in peak structure in the Stokes and current. By comparing solid lines in Figs. 2(a) and 4(a), one sees the absence versus presence of the two-peak structure in the region from -20 to -15 at

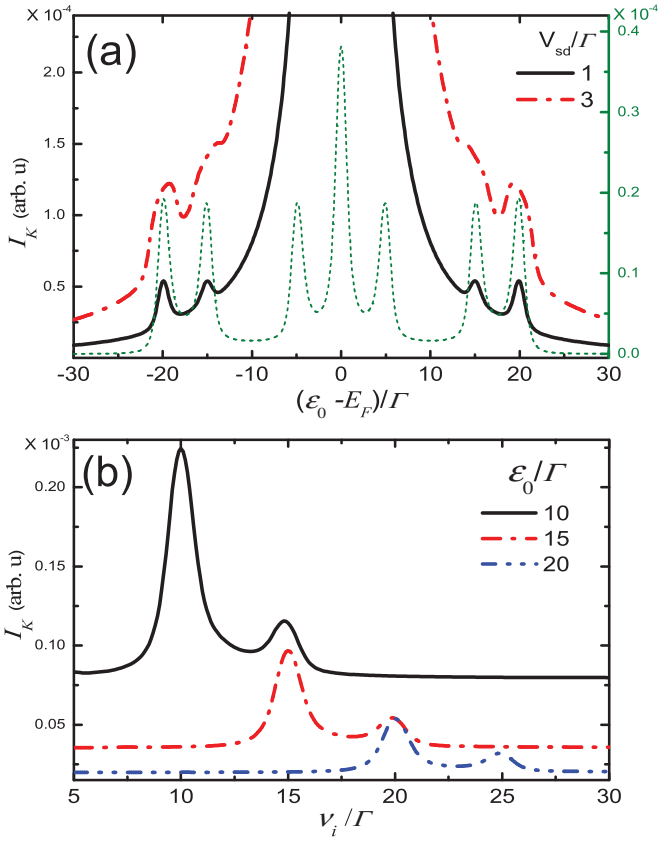

FIG. 4. (Color online) Electric current averaged over period of oscillation [Eqs. (43)–(46)] shown as function of (a) molecular level position ε_0 at bias $V_{sd} = 1$ (solid line, black) and 3 (dashed-dotted line, red), and (b) incident laser filled frequency ν_i at level position $\varepsilon_0 = 10$ (solid line, black), 15 (dashed-dotted line, red), and 20 (dashed-double dotted line, blue). Dotted line (green) in panel (a) shows current without I_K^i contribution [Eq. (43)] at $V_{sd} = 1$. See text for parameters.

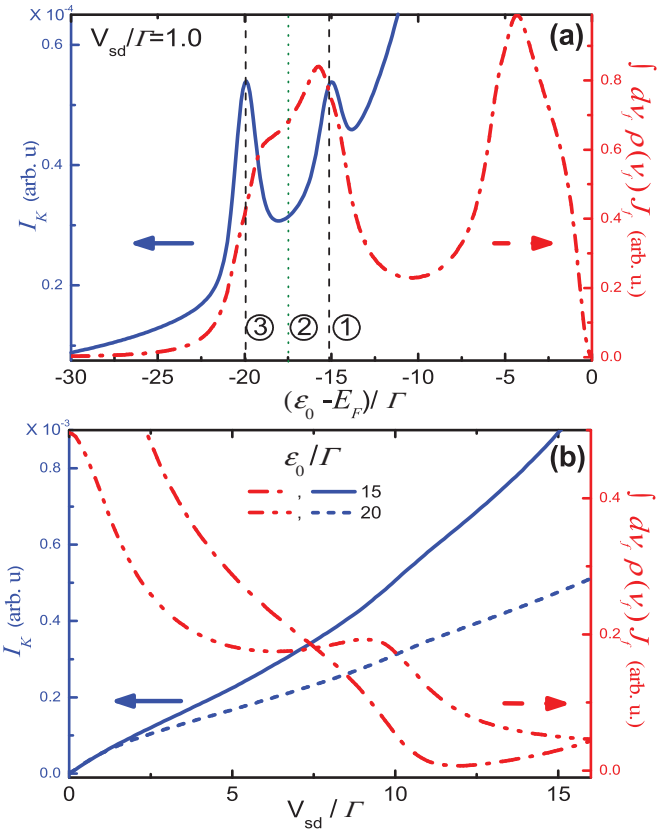

FIG. 6. (Color online) Stokes intensity averaged over period of oscillation of the photon flux (red) [Eq. (40)] and time-averaged current (blue) [Eqs. (43)–(46)] as functions of (a) position of the molecular level ε_0 at $V_{sd} = 1$ (Stokes: dashed-dotted line; current: solid line) and (b) bias V_{sd} at the level positions $\varepsilon_0 = 15$ (Stokes: dashed-dotted line; current: solid line) and 20 (Stokes: dashed-double-dotted line; current: dashed line). Vertical dashed lines in panel (a) are used as a guide to the eye. See text for parameters.

low biases $V_{sd} < \Gamma$ [for convenience, also the current without dominant contribution I_K^i is presented in Fig. 4(a) as dotted line].

Figure 4(b) demonstrates the dependence of the current on frequency of the incident laser field. The structure is similar to the usual resonant inelastic conductance plots with two peaks representing elastic (ε_0 crosses chemical potential) and

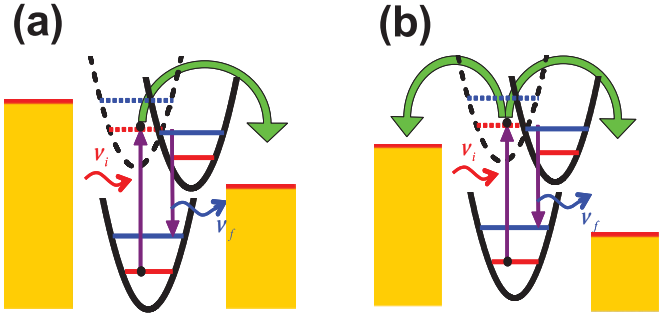

FIG. 5. (Color online) Sketches of Raman scattering process of the type presented in Fig. 3(b) (a) with and (b) without contribution to current through the junction.

first vibrational sideband ($\varepsilon_0 + \omega_v$ crosses chemical potential) contributions. This figure is similar to the Stokes intensity plot in Fig. 2(b). Once more, the difference in contributions to the Stokes signal and current sketched in Fig. 5 explain the difference in structure of the peaks in Figs. 2(b) and 4(b), respectively.

Finally, we discuss the possible fluctuations of the Stokes and current resulting from fluctuations of underlying driving parameters: position of the level and bias. Note that since the conductance in experiments is measured as the current at low bias, we can use our results for qualitative comparison to correlation between conductance and Stokes presented in Ref. 15. The latter work explains this temporal behavior by molecular geometry reorganization. While such an explanation is very reasonable, and indeed might be the main source of the observed correlated behavior, we propose an alternative mechanism for the effect.

Figure 6(a) compares the dependence of Stokes and current on position of the level [see Figs. 2(a) and 4(a)]. Since the problem is particle-hole symmetric, we show only half of the energy region ($\varepsilon_0 < E_F$). As is discussed above, processes

shown in Fig. 5 contribute differently to current and Stokes, which results in a valley in the current curve (solid line, blue) around $\varepsilon_0 = -17.5$ and the absence of such a valley in the Stokes curve (dashed-dotted line, red). Consequently, fluctuations of position of molecular level in this region may lead to a different response in measured Stokes and conductance. In Fig. 6(a), vertical dashed lines are used as a guide to the eye to show two possibilities: shift of the molecular level closer to Fermi energy may lead to either a decrease in both Stokes and conductance signals or a decrease in Stokes with simultaneous increase in conductance. Therefore, we can speculate that, for highest occupied molecular orbital (HOMO) residing around $E_F - \nu_i + \omega_v$ (or LUMO around $E_F + \nu_i - \omega_v$), for weak molecule-contact coupling, one may expect observing correlated (and anticorrelated) response of Stokes intensity and conductance caused by environmental fluctuations.

Similarly, a different response of Stokes and conductance may stem from bias fluctuations. Figure 6(b) shows dependence of Stokes and current versus bias for two positions of molecular level. Regions of (anti)correlations of the two signals resulting from bias fluctuations are easily identifiable in this plot.

Figure 7 shows correlation (a) and anticorrelation (b) of Stokes and current as functions of time. We calculate time dependence of Stokes intensity and current (both averaged over the period of oscillation) resulting from instantaneous shifts of molecular levels at $t = 0$. Three different molecular level positions at -15, -17.5, and -20 are denoted by ①, ②, and ③, respectively, in Fig. 6(a). The same notation is used in Fig. 7. For the molecular level shift ① → ②, both Stokes and current signals decrease together [see Fig. 7(a)], while shift ② → ③ leads to the anticorrelated response [see Fig. 7(b)]. Analytical forms for the time-dependent Stokes intensity and current due to the molecular level shift are presented in the Appendix. Thus, our simple model provides a specific mechanism for temporal (anti)correlation between Stokes signal and conductance, which may be responsible for at least part of the experimentally observed temporal correlation phenomena.[15]

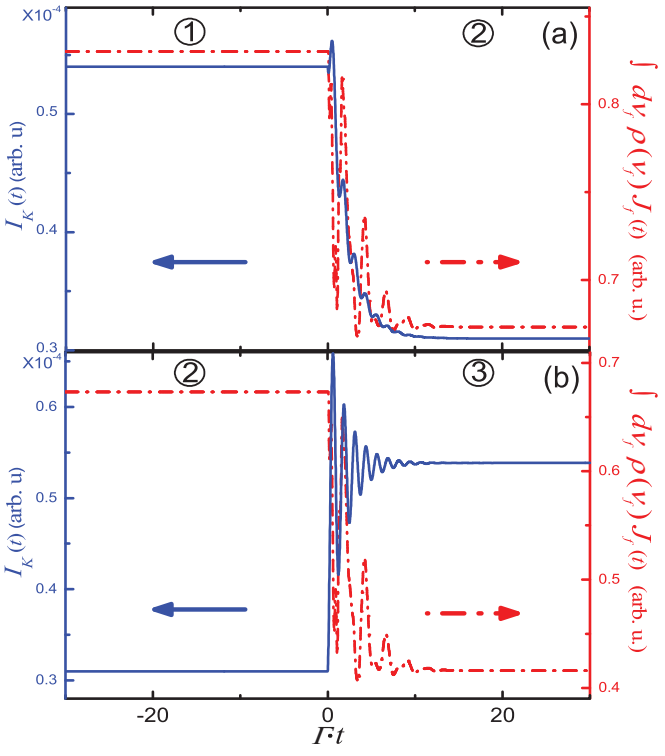

FIG. 7. (Color online) Response of Stokes intensity (dashed-dotted line, red) and current (solid line, blue), both averaged over period of oscillation of the corresponding flux, to instant shift of the molecular level shown as function of time. The molecular level is shifted (a) from ① (-15) to ② (-17.5) at $t = 0$ (correlation), and (b) from ② (-17.5) to ③ (-20) at $t = 0$ (anticorrelation). The three molecular level positions ①, ②, and ③ are denoted as vertical dashed lines in Fig. 6(a).

V. CONCLUSION

We consider a time-dependent variant of the charge-transfer SERS model[8] previously generalized to steady-state situations.[30] Contrary to previous considerations, our approach treats coupling to incident laser field nonperturbatively, which (together with the possibility of consideration of arbitrary time dependence of incident pulse) paves a way to realistic simulations of Raman spectroscopy experiments in molecular junctions. After formulating general theory, we restrict our consideration to harmonic driving. This allows us to derive expressions for Raman flux and current analytically.

Since both electrons and photons are involved in the same Raman scattering process, characteristic features of the two fluxes (Raman photon flux and conductance) should at least partially resemble each other. We use this argument to demonstrate within the model similarity of dependence of the two fluxes on external parameters (position of molecular level, applied bias, and incident field frequency). The Feynman diagrams responsible for the proposed similarity are identified.

We demonstrate that, due to the presence of Fermi populations in the contacts, the charge flux resulting from electrons participating in the Raman scattering has characteristic features specific to the electron flux only. In particular, for weak coupling ($\Gamma < V_{sd}$), current dependence on position of the molecular level has a two-peak structure in the region $\varepsilon_0 - E_F \sim \pm(\nu_i - \omega_v)$. Absence of such a structure for Stokes signal in the same region allows for the same (or opposite) response to fluctuations in the position of the molecular level. Similarly, correlated (or anticorrelated) behavior can be found in response to bias fluctuations. These findings may serve as an alternative (to configurational change in molecular structure) explanation to at least part of (anti)correlated temporal behavior of Stokes signal and conductance reported in Ref. 15.

Extension of the theory to description of molecular junction responses in the language of molecular states, incorporation of local fields (e.g., simulated for junction geometry within a finite-difference time-domain approach) as realistic driving force, and application of the theory to realistic simulations is the goal of future research.

ACKNOWLEDGMENTS

We gratefully acknowledge support by the National Science Foundation (CHE-1057930), the US-Israel Binational Science

Foundation (Grant No. 2008282), and the Hellman Family Foundation.

APPENDIX: INSTANT LEVEL SHIFT WITH EXTERNAL HARMONIC DRIVING

Analytical expressions for current within the resonant level model were derived in Ref. 33 for two separate cases: (i) instant level shift and (ii) harmonic driving. Here, we present a similar derivation for the case when both effects are present simultaneously.

Analytic expressions for projections of the single-particle Green's function [Eq. (15)] for instantaneous shift of the molecular level from ε_0 to $\varepsilon_0+\Delta$ at $t=0$ driven by harmonic incident field are

$$G^r(t,t') = -i\theta(t-t')\exp\left[-i\left(\varepsilon_0 - i\frac{\Gamma}{2}\right)(t-t') - i\Delta[\theta(t)t - \theta(t')t'] - i\frac{C}{\nu_i}[\sin(\nu_i t) - \sin(\nu_i t')]\right], \tag{A1}$$

$$\begin{aligned} G^{\lessgtr}(t,t') = &\sum_{k_1,k_2=-\infty}^{\infty} J_{k_1}\left(\frac{C}{\nu_i}\right) J_{k_2}\left(\frac{C}{\nu_i}\right)\int\frac{dE}{2\pi}\Sigma^{\lessgtr}_{L+R}(E)\exp\left(-iE(t-t') - i\frac{C}{\nu_i}[\sin(\nu_i t) - \sin(\nu_i t')]\right)\\ &\times\frac{e^{i\nu_i k_1 t}}{E-\varepsilon_0-\theta(t)\Delta - k_1\nu_i + i\frac{\Gamma}{2}}\left[1-\theta(t)\frac{\Delta e^{i(E-\varepsilon_0-\Delta-\nu_i k_1+i\Gamma/2)t}}{E-\varepsilon_0-\nu_i k_1+i\frac{\Gamma}{2}}\right]\\ &\times\frac{e^{-i\nu_i k_2 t'}}{E-\varepsilon_0-\theta(t')\Delta - k_2\nu_i - i\frac{\Gamma}{2}}\left[1-\theta(t')\frac{\Delta e^{-i(E-\varepsilon_0-\Delta-\nu_i k_2-i\Gamma/2)t'}}{E-\varepsilon_0-\nu_i k_2-i\frac{\Gamma}{2}}\right]. \end{aligned} \tag{A2}$$

For $t,t'<0$, Eqs. (A1) and (A2) reduce to (37) and (38), respectively.

Substituting (A1) and (A2) into the retarded projection of (24), and performing right-side Fourier transform (41) of the resulting expression leads to Eq. (42) for $t<0$ and to

$$\begin{aligned} P^r(t,\omega) = -i&\sum_{k_1,k_2=-\infty}^{+\infty} J_{k_1}\left(\frac{C}{\nu_i}\right) J_{k_2}\left(\frac{C}{\nu_i}\right)\int\frac{dE}{2\pi}\Sigma^{<}_{L+R}(E)\left(1-\Delta\frac{e^{-i(E-\varepsilon_0-\Delta-\nu_i k_2-i\Gamma/2)t}}{E-\varepsilon_0-\nu_i k_2-i\frac{\Gamma}{2}}\right)\\ &\times\frac{\exp\{i\,[\nu_i(k_1-k_2)-\omega]\,t\}}{\left[E-\varepsilon_0-\Delta-\nu_i k_1+i\frac{\Gamma}{2}\right]\left[E-\varepsilon_0-\Delta-\nu_i k_2-i\frac{\Gamma}{2}\right]\left[E-\varepsilon_0-\Delta-\nu_i k_1+\omega+i\frac{\Gamma}{2}\right]}\\ &\times\left\{1-e^{i(E-\varepsilon_0-\Delta-\nu_i k_1+\omega+i\Gamma/2)t}\left[1-\frac{1-e^{-i\omega t}}{\omega}\Delta\left(1+\frac{\omega-\Delta}{E-\varepsilon_0-\nu_i k_1+i\frac{\Gamma}{2}}\right)\right.\right.\\ &\left.\left.\times - e^{-i\Delta t}\left(1-\frac{\Delta}{E-\varepsilon_0-\nu_i k_1+i\frac{\Gamma}{2}}\right)\left(1-\frac{\Delta}{E-\varepsilon_0-\nu_i k_1+\omega+i\frac{\Gamma}{2}}\right)\right]\right\} + (\omega\to-\omega)^* \end{aligned} \tag{A3}$$

for $t>0$. Note that Eq.(A3) reduces to the form of Eq. (42) with $\varepsilon_0\to\varepsilon_0+\Delta$ when $t\to+\infty$. Time-dependent Raman flux can be obtained from Eq. (40) substituting (42) and (A3) for $t<0$ and $t>0$, respectively. As the time-dependent Raman is averaged over the period of oscillation at asymptote $t\to+\infty$, transient time dependency of the resulting expression still remains. It decays on a time scale of $1/\Gamma$.

Time-dependent current is obtained by substituting (A1) into (35), changed for $t>0$ from Eqs. (43)–(46). By neglecting fast oscillating terms, current components averaged over period of oscillation at asymptote are

$$\begin{aligned} \left\langle I^i_K(t)\right\rangle = 2\sum_{\xi}\int\frac{dE}{2\pi}&\left\{e^{-\frac{\Gamma}{2}t}\left|\sum_k\frac{J_k\left(\frac{C}{\nu_i}\right)J_{k-\xi}\left(\frac{C}{\nu_i}\right)}{E-\varepsilon_0+(\xi-k)\nu_i+i\frac{\Gamma}{2}}\right|^2 + \left(1-e^{-\frac{\Gamma}{2}t}\right)\left|\sum_k\frac{J_k\left(\frac{C}{\nu_i}\right)J_{k-\xi}\left(\frac{C}{\nu_i}\right)}{E-\varepsilon_0-\Delta+(\xi-k)\nu_i+i\frac{\Gamma}{2}}\right|^2\right\}\\ &\times[\Sigma^<_K(E)\Sigma^>_{\bar K}(E+\xi\nu_i) - \Sigma^<_{\bar K}(E)\Sigma^>_K(E+\xi\nu_i)], \end{aligned} \tag{A4}$$

$$\begin{aligned} \left\langle I^{i\nu}_K(t)\right\rangle = 2|M_v|^2\sum_{\xi}\int\frac{dE}{2\pi}&\left\{N_v\left[e^{-\frac{\Gamma}{2}t}\Lambda^0_\xi(\omega_v,E) + \left(1-e^{i\omega_v t}e^{-\frac{\Gamma}{2}t}\right)\Lambda^\Delta_\xi(\omega_v,E)\right]\right.\\ &\times[\Sigma^<_K(E)\Sigma^>_{\bar K}(E+\omega_v+\xi\nu_i) - \Sigma^<_{\bar K}(E)\Sigma^>_K(E+\omega_v+\xi\nu_i)]\\ &+[N_v+1]\left[e^{-\frac{\Gamma}{2}t}\Lambda^0_\xi(-\omega_v,E) + (1-e^{-i\omega_v t}e^{-\frac{\Gamma}{2}t})\Lambda^\Delta_\xi(-\omega_v,E)\right]\\ &\left.\times[\Sigma^<_K(E)\Sigma^>_{\bar K}(E-\omega_v+\xi\nu_i) - \Sigma^<_{\bar K}(E)\Sigma^>_K(E-\omega_v+\xi\nu_i)]\right\}, \end{aligned} \tag{A5}$$

$$\left\langle I_K^{if}(t)\right\rangle = 2|M_f|^2 \sum_\xi \int_0^\infty d\nu_f\, \rho(\nu_f) \int \frac{dE}{2\pi} \left[e^{-\frac{\Gamma}{2}t}\Lambda_\xi^0(-\nu_f,E) + \left(1-e^{-i\nu_f t}e^{-\frac{\Gamma}{2}t}\right)\Lambda_\xi^\Delta(-\nu_f,E)\right]$$
$$\times[\Sigma_K^<(E)\Sigma_{\bar K}^>(E-\nu_f+\xi\nu_i) - \Sigma_{\bar K}^<(E)\Sigma_K^>(E-\nu_f+\xi\nu_i)], \tag{A6}$$

$$\left\langle I_K^{i\nu f}(t)\right\rangle = 2|M_v|^2\,|M_f|^2 \mathrm{Re}\sum_\xi \int_0^\infty d\nu_f\, \rho(\nu_f)$$
$$\times \int \frac{dE}{2\pi}\Big\{N_v\Big[e^{-\frac{\Gamma}{2}t}\Phi_\xi^0(\omega_v,-\omega_v,E) + \left(1-e^{i(2\omega_v-\nu_f)t}e^{-\frac{\Gamma}{2}t}\right)\Phi_\xi^\Delta(\omega_v,-\omega_v,E)$$
$$+e^{-\frac{\Gamma}{2}t}\Phi_\xi^0(\omega_v,\nu_f,E) + \left(1-e^{i(\omega_v-2\nu_f)t}e^{-\frac{\Gamma}{2}t}\right)\Phi_\xi^\Delta(\omega_v,\nu_f,E)\Big]$$
$$\times[\Sigma_K^<(E)\Sigma_{\bar K}^>(E+\omega_v-\nu_f+\xi\nu_i) - \Sigma_{\bar K}^<(E)\Sigma_K^>(E+\omega_v-\nu_f+\xi\nu_i)]$$
$$+[N_v+1]\Big[e^{-\frac{\Gamma}{2}t}\Phi_\xi^0(-\omega_v,\omega_v,E) + \left(1-e^{-i(2\omega_v+\nu_f)t}e^{-\frac{\Gamma}{2}t}\right)\Phi_\xi^\Delta(-\omega_v,\omega_v,E)$$
$$+\,e^{-\frac{\Gamma}{2}t}\Phi_\xi^0(-\omega_v,\nu_f,E) + \left(1-e^{-i(\omega_v+2\nu_f)t}e^{-\frac{\Gamma}{2}t}\right)\Phi_\xi^\Delta(-\omega_v,\nu_f,E)\Big]$$
$$\times[\Sigma_K^<(E)\Sigma_{\bar K}^>(E-\omega_v-\nu_f+\xi\nu_i) - \Sigma_{\bar K}^<(E)\Sigma_K^>(E-\omega_v-\nu_f+\xi\nu_i)]\Big\}, \tag{A7}$$

where $\bar K$ stands for the alternative to the K choice of the interface, $\Lambda_\xi^0(x,E)$ and $\Phi_\xi^0(x,y,E)$ are defined in Eqs. (47) and (48), respectively. Definition of $\Lambda_\xi^\Delta(x,E)$ and $\Phi_\xi^\Delta(x,y,E)$ is similar with $\varepsilon_0 \to \varepsilon_0+\Delta$.

*t7park@ucsd.edu
†migalperin@ucsd.edu

[1] D. L. Jeanmaire and R. VanDuyne, J. Electroanal. Chem. **84**, 1 (1977).
[2] S. Nie and S. R. Emory, Science **279**, 1102 (1997).
[3] K. Kneipp, Y. Wang, H. Kneipp, L. T. Perelman, I. Itzkan, R. R. Dasari, and M. S. Feld, Phys. Rev. Lett. **78**, 1667 (1997).
[4] J. Jiang, K. Bosnick, M. Maillard, and L. Brus, J. Phys. Chem. B **107**, 9964 (2003).
[5] K. A. Willets and R. VanDuyne, Annu. Rev. Phys. Chem. **58**, 267 (2007).
[6] J. Gersten and A. Nitzan, J. Chem. Phys. **73**, 3023 (1980).
[7] J. I. Gersten, R. L. Birke, and J. R. Lombardi, Phys. Rev. Lett. **43**, 147 (1979).
[8] B. N. J. Persson, Chem. Phys. Lett. **82**, 561 (1981).
[9] A. C. Albrecht, J. Chem. Phys. **34**, 1476 (1961).
[10] J. R. Lombardi, R. L. Birke, L. A. Sanchez, I. Bernard, and S. C. Sun, Chem. Phys. Lett. **104**, 240 (1984).
[11] J. R. Lombardi, R. L. Birke, T. Lu, and J. Xu, J. Chem. Phys. **84**, 4174 (1986).
[12] J. R. Lombardi and R. L. Birke, J. Chem. Phys. **126**, 244709 (2007).
[13] J. R. Lombardi and R. L. Birke, J. Phys. Chem. C **112**, 5605 (2008).
[14] A. M. Kelley, J. Chem. Phys. **128**, 224702 (2008).
[15] D. R. Ward, N. J. Halas, J. W. Ciszek, J. M. Tour, Y. Wu, P. Nordlander, and D. Natelson, Nano Lett. **8**, 919 (2008).
[16] D. R. Ward, D. A. Corley, J. M. Tour, and D. Natelson, Nat. Nanotechnol. **6**, 33 (2011).
[17] Z. Ioffe, T. Shamai, A. Ophir, G. Noy, I. Yutsis, K. Kfir, O. Cheshnovsky, and Y. Selzer, Nat. Nanotechnol. **3**, 727 (2008).
[18] N. B. Zhitenev, H. Meng, and Z. Bao, Phys. Rev. Lett. **88**, 226801 (2002).
[19] B. J. LeRoy, S. G. Lemay, J. Kong, and C. Dekker, Nature (London) **432**, 371 (2004).
[20] A. Bayman, P. K. Hansma, and W. C. Kaska, Phys. Rev. B **24**, 2449 (1981).
[21] J. R. Hahn, H. J. Lee, and W. Ho, Phys. Rev. Lett. **85**, 1914 (2000).
[22] W. Wang, T. Lee, I. Kretzschmar, and M. A. Reed, Nano Lett. **4**, 643 (2004).
[23] R. H. M. Smit, Y. Noat, C. Untiedt, N. D. Lang, M. C. van Hemert, and J. M. van Ruitenbeek, Nature (London) **419**, 906 (2002).
[24] N. Agrait, C. Untiedt, G. Rubio-Bollinger, and S. Vieira, Phys. Rev. Lett. **88**, 216803 (2002).
[25] D. Djukic and J. M. van Ruitenbeek, Nano Lett. **6**, 789 (2006).
[26] S. Mukamel, *Principles of Nonlinear Optical Spectroscopy*. (Oxford University Press, New York, 1995).
[27] M. Galperin, M. A. Ratner, and A. Nitzan, Nano Lett. **9**, 758 (2009).
[28] M. Galperin, M. A. Ratner, and A. Nitzan, J. Chem. Phys. **130**, 144109 (2009).
[29] G. Li and A. Nitzan (unpublished).
[30] M. Oren, A. Nitzan, and M. Galperin (to be published).
[31] M. Esposito and M. Galperin, Phys. Rev. B **79**, 205303 (2009).
[32] M. Esposito and M. Galperin, J. Phys. Chem. C **114**, 20362–20369 (2010).
[33] A.-P. Jauho, N. S. Wingreen, and Y. Meir, Phys. Rev. B **50**, 5528 (1994).
[34] M. P. Anantram and S. Datta, Phys. Rev. B **51**, 7632 (1995).
[35] B. Wang, J. Wang, and H. Guo, Phys. Rev. Lett. **82**, 398 (1999).
[36] M. Wagner, Phys. Rev. B **44**, 6104 (1991).
[37] P. Myöhänen, A. Stan, G. Stefanucci, and R. van Leeuwen, J. Phys.: Conf. Ser. **220**, 012017 (2010).

[38]M. Sukharev and M. Galperin, Phys. Rev. B **81**, 165307 (2010).
[39]B. D. Fainberg, M. Sukharev, T.-H. Park, and M. Galperin, Phys. Rev. B **83**, 205425 (2011).
[40]M. Galperin, A. Nitzan, and M. A. Ratner, Phys. Rev. B **78**, 125320 (2008).
[41]G. D. Mahan, *Many-Particle Physics* (Plenum, New York, 1990).
[42]M. Galperin, A. Nitzan, and M. A. Ratner, Phys. Rev. B **75**, 155312 (2007).
[43]A. Ueda, O. Entin-Wohlman, M. Eto, and A. Aharony, e-print arXiv:1008.5195.
[44]H. Haug and A.-P. Jauho, *Quantum Kinetics in Transport and Optics of Semiconductors* (Springer, Berlin, 1996).
[45]D. R. Ward, N. K. Grady, C. S. Levin, N. J. Halas, Y. Wu, P. Nordlander, and D. Natelson, Nano Lett. **7**, 1396 (2007).
[46]I. S. Gradshteyn and I. M. Ryzhik, *Table of Integrals, Series, and Products* (Academic, San Diego, 2007).